

X-ray Bright Optically Inactive Galaxies in XMM-Newton/SDSS fields: more diluted than absorbed?

I. Georgantopoulos & A. Georgakakis

Institute of Astronomy & Astrophysics, National Observatory of Athens, I. Metaxa & B. Pavlou, 15236, Athens, Greece

22 August 2018

ABSTRACT

We explore the properties of X-ray Bright Optically Inactive Galaxies (XBONG) detected in the 0.5–8 keV spectral band in 20 public *XMM-Newton* fields overlapping with the SDSS. We constrain our sample to optically extended systems with $\log f_X/f_{opt} > -2$ that have spectroscopic identifications available from the SDSS ($r < 19.2$ mag). The resulting sample contains 12 objects with $L_X(0.5 - 8 \text{ keV}) = 5 \times 10^{41} - 2 \times 10^{44} \text{ erg s}^{-1}$ in the redshift range $0.06 < z < 0.45$. The X-ray emission in four cases is extended suggesting the presence of hot gas associated with a cluster or group of galaxies. The X-ray spectral fits show that two additional sources are best fit with a thermal component emission ($kT \sim 1 \text{ keV}$). Three sources are most likely associated with AGN: their X-ray spectrum is described by a steep photon index $\Gamma \sim 1.9$ typical of unobscured AGN while, they are very luminous in X-rays ($L_X(0.5 - 8 \text{ keV}) \approx 10^{43} - 10^{44} \text{ erg s}^{-1}$). Finally, three more sources could be associated with either normal galaxies or unobscured Low Luminosity AGN ($L_X < 10^{42} \text{ erg s}^{-1}$). We find no evidence for significant X-ray absorbing columns in any of our XBONGs. The above suggest that XBONGs, selected in the total 0.5–8 keV band, comprise a mixed bag of objects primarily including normal elliptical galaxies and type-1 AGN whose optical nuclear spectrum is probably diluted by the strong stellar continuum. Nevertheless, as our sample is not statistically complete we cannot exclude the possibility that a fraction of optically fainter XBONG may be associated with heavily obscured AGN.

Key words: Galaxies: active – Quasars: general – X-rays: general

1 INTRODUCTION

Deep *Chandra* surveys have resolved the bulk of the X-ray background in both the soft and the hard energies (Mushotzky et al. 2000; Brandt et al. 2001; Giacconi et al. 2002; Alexander et al. 2003). A striking result is that these surveys do not find a single dominant population of heavily obscured AGNs, predicted by the X-ray background population synthesis models. On the contrary a heterogeneous population of sources is detected comprising a mix of (i) BL AGN (QSOs and Seyfert-1 galaxies), (ii) narrow emission line AGN, (iii) optically faint sources ($I > 24$ mag) and (iv) ‘passive’ galaxies with absorption line optical spectra. The latter class of sources, frequently dubbed X-ray Bright Optically Inactive Galaxies (XBONGs), shows no sign of AGN activity in their optical spectra (e.g. no emission lines), while the X-ray luminosity is large enough ($\gtrsim 10^{42} \text{ erg s}^{-1}$) that is hard to reconcile without invoking the presence of AGN activity (Fiore et al. 2003; Hornschemeier et al. 2001; Barger et al. 2001). Although this class of sources has been detected in previous low resolution X-ray missions (Elvis et al. 1981; Griffiths et al. 1995; Moran et al. 1996; Blair, Geor-

gantopoulos & Stewart 1997) it is only recently that they have received much attention. This interest has been initiated by the suggestion that these sources host heavily obscured AGNs (e.g. Comastri et al. 2002) and therefore, they may be the missing link between observations and model predictions. Indeed, a large fraction of completely hidden AGNs may be hosted by optically normal galaxies, partially explaining the scarcity of obscured AGN in deep X-ray surveys (Comastri et al. 2002).

Alternatively, the lack of optical emission lines can be explained if the nuclear component is outshined by the strong stellar continuum (e.g. Severgnini et al. 2003). The X-ray spectra provide an invaluable tool for discriminating between the above possibilities. Unfortunately, the sources detected in the deep *Chandra* fields are in general too faint to allow detailed X-ray spectral analysis.

Therefore, it is important to find nearby, bright examples of XBONGs in wide angle relatively shallower surveys. Wide areal coverage is difficult to achieve with the *Chandra* observatory due its limited field-of-view. On the contrary, *XMM-Newton* with 4 times larger field-of-view provides an ideal platform for such a study. In this paper we

exploit the capabilities and the large volume of archival data of the *XMM-Newton* to serendipitously identify XBONGs in public fields selected to overlap with the Sloan Digital Sky Survey (SDSS; York et al. 2000). This is to exploit the superb and uniform 5-band optical photometry and spectroscopy available in this area. Throughout this paper we adopt $H_0 = 65 \text{ km s}^{-1} \text{ Mpc}^{-1}$ and $\Omega_M = 0.3$, $\Omega_\Lambda = 0.7$.

2 THE DATA

2.1 The SDSS data

In this paper we use *XMM-Newton* archival observations with a proprietary period that expired before September 2003 and that overlap with the first data release of the SDSS (DR1; Stoughton et al. 2002). The SDSS is an ongoing imaging and spectroscopic survey that aims to cover about $10,000 \text{ deg}^2$ of the sky. Photometry is performed in 5 bands (*ugriz*; Fukugita et al. 1996; Stoughton et al. 2002) to the limiting magnitude $g \approx 23$ mag, providing a uniform and homogeneous multi-color photometric catalogue. The SDSS spectroscopic observations will obtain spectra for over 1 million objects, including galaxies brighter than $r = 17.7$ mag, luminous red galaxies to $z \approx 0.45$ and colour selected QSOs (York et al. 2000; Stoughton et al. 2002).

2.2 The *XMM-Newton* data

The *XMM-Newton* archival observations used here have the EPIC (European Photon Imaging Camera; Strüder et al. 2001; Turner et al. 2001) cameras as the prime instrument operated in full frame mode. For fields observed more than once with the *XMM-Newton* we use the deeper of the multiple observations. The total of 20 *XMM-Newton* fields used here are listed in Table 1.

The X-ray data have been analysed using the Science Analysis Software (SAS 5.4). The event files produced by the *XMM-Newton* Science Center data reduction pipeline were screened for high particle background periods by rejecting time intervals with 0.5–10 keV count rates higher than 30 and 15 cts/s for the PN and the two MOS cameras respectively. The PN and MOS good time intervals for these pointings are shown in Table 1. The differences between the PN and MOS exposure times are due to varying start and end times of individual observations. Only events corresponding to patterns 0–4 for the PN and 0–12 for MOS have been kept.

In order to increase the signal-to-noise ratio and to reach fainter fluxes the PN and the MOS event files have been combined into a single event list using the MERGE task of SAS. Images have been extracted in the spectral bands 0.5–8 (total), 0.5–2 (soft) and 2–8 keV (hard) for both the merged and the individual PN and MOS event files. We use the more sensitive (higher S/N ratio) merged image for source extraction and flux estimation, while the individual PN and MOS images are used to calculate hardness ratios. This is because the interpretation of hardness ratios is simplified if the extracted count rates are from one detector only. Exposure maps accounting for vignetting, CCD gaps and bad pixels have been constructed for each spectral band. In the present study the source detection is per-

formed on the 0.5–8 keV image using the EWAVELET task of SAS with a detection threshold of 5σ . In this paper we only consider sources with offaxis angles $< 13.5 \text{ arcmin}$ and therefore the total surveyed area is about 3.14 deg^2 . A total of 1286 X-ray sources have been detected to the limit $f_X(0.5 - 8 \text{ keV}) \approx 2 \times 10^{-15} \text{ erg s}^{-1} \text{ cm}^{-2}$. About 10 per cent of the total survey area is covered at the flux limit $f_X(0.5 - 8 \text{ keV}) \approx 3 \times 10^{-15} \text{ erg s}^{-1} \text{ cm}^{-2}$. This fraction increases to about 50 per cent at $\approx 7 \times 10^{-15} \text{ erg s}^{-1} \text{ cm}^{-2}$.

Count rates in the merged (PN+MOS) images as well as the individual PN and MOS images are estimated within an 18 arcsec aperture. For the background estimation we use the background maps generated as a by-product of the EWAVELET task of SAS. A small fraction of sources lie close to masked regions (CCD gaps or hot pixels) on either the MOS or the PN detectors. This may introduce errors in the estimated source counts. To avoid this bias, the source count rates (and hence the hardness ratios and the flux) are estimated using the detector (MOS or PN) with no masked pixels in the vicinity of the source.

We convert counts to flux assuming a power-law spectrum with $\Gamma = 1.7$ and the appropriate Galactic absorption for each field listed in Table 1 (Dickey & Lockman 1990). The mean count-rate to flux conversion (or Energy Conversion Factor, ECF) for the mosaic of all three detectors is estimated by weighting the ECFs of individual detectors by the respective exposure time. For the encircled energy correction, accounting for the energy fraction outside the aperture within which source counts are accumulated, we adopt the calibration given by the *XMM-Newton* Calibration Documentation ^{*}.

3 THE SAMPLE

The SDSS optical photometric catalogue is used to identify optical counterparts to the X-ray sources by estimating the probability, P , that a given candidate is a chance coincidence (Downes et al. 1986). The probability depends on both the separation of the optical counterpart from the X-ray centroid and the surface density of the optical sources at the given magnitude (see Georgakakis et al. 2004 for details). For our identifications we adopt a probability threshold $P < 0.015$ and a maximum search radius of 7 arcsec.

We are further selecting sources which (i) are associated with galaxies i.e. they are optically extended sources according to the SDSS star-galaxy classification and (ii) have optical SDSS spectra available. A total of 33 sources fulfill the above criteria of which 14 have ‘early-type’ spectra showing absorption lines only and lacking emission lines. Finally, we exclude two sources which have low X-ray to optical flux ratio, $\log f_X/f_{opt} < -2$ and therefore are most probably associated with ‘normal’ galaxies i.e. their X-ray emission comes from binaries and diffuse hot gas (see Hornschemeier et al. 2003). Both these sources are detected at the vicinity of the cluster Abell2670, having a redshift of $z=0.07$, and are most likely associated with the above cluster. Their X-ray coordinates (J2000) are $\alpha = 23^h 53^m 40.5^s$, $\delta =$

^{*} http://xmm.vilspa.esa.es/external/xmm_sw_cal/calib/documentation.shtml#XRT

RA (J2000)	Dec (J2000)	FILTER	N _H (10 ²⁰ cm ⁻²)	PN exp. time (sec)	MOS1 exp. time (sec)	Field name
23 54 09	-10 24 00	MEDIUM	2.91	13 600	19 100	ABELL 2670
23 37 40	+00 16 33	THIN	3.82	8 200	13 300	RXCJ 2337.6+0016
17 01 23	+64 14 08	MEDIUM	2.65	2 300	3 900	RXJ 1701.3
15 43 59	+53 59 04	THIN	1.27	14 200	19 200	SBS 1542+541
13 49 15	+60 11 26	THIN	1.80	14 100	18 100	NGC 5322
13 04 12	+67 30 25	THIN	1.80	14 600	17 100	ABELL 1674
12 45 09	+00 27 38	MEDIUM	1.73	46 300	55 500	NGC 4666
12 31 32	+64 14 21	THIN	1.98	26 100	30 100	MS 1229.2+6430
09 35 51	+61 21 11	THIN	2.70	20 400	33 900	UGC 5051
09 34 02	+55 14 20	THIN	1.98	23 500	28 500	IZW 18
09 17 53	+51 43 38	MEDIUM	1.44	15 900	13 600	ABELL 773
08 31 41	+52 45 18	MEDIUM	3.83	66 800	73 300	APM 08279+5255
03 57 22	+01 10 56	THIN	13.20	19 100	21 400	HAWAII 167
03 38 29	+00 21 56	THIN	8.15	8 900	6 700	SDSS 033829.31+00215
03 02 39	+00 07 40	THIN	7.16	38 100	46 900	CFRS 3H
02 56 33	+00 06 12	THIN	6.50	—	11 600	RX J0256.5+0006
02 41 05	-08 15 21	MEDIUM	3.07	12 300	15 600	NGC 1052
01 59 50	+00 23 41	MEDIUM	2.65	3 800	—	MRK 1014
01 52 42	+01 00 43	MEDIUM	2.80	5 800	17 200	ABELL 267
00 43 20	-00 51 15	MEDIUM	2.33	15 700	—	UM 269

Table 1. The archival *XMM-Newton* pointings used in this study.

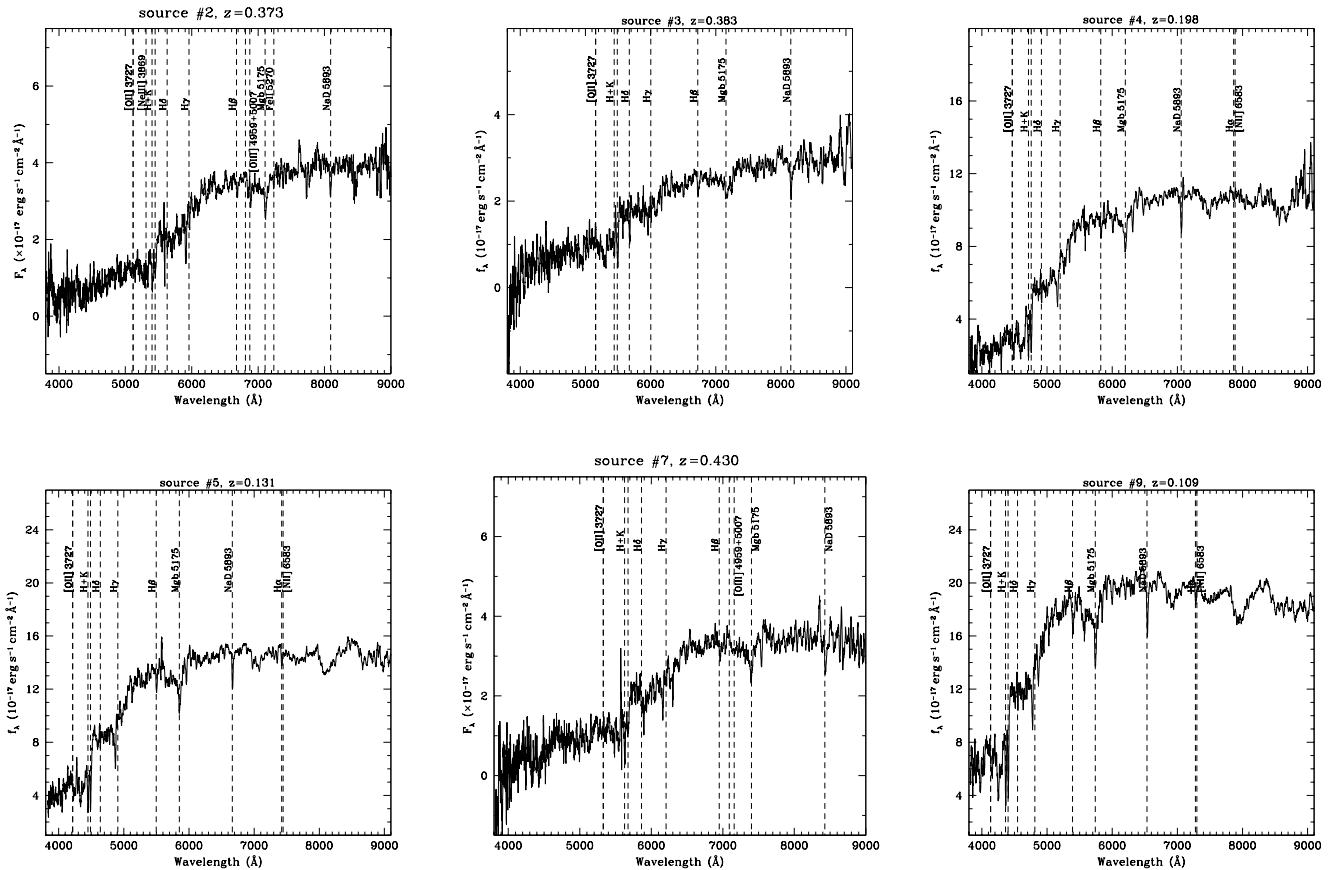


Figure 1. The optical spectra of the six sources that are likely to be associated with AGN.

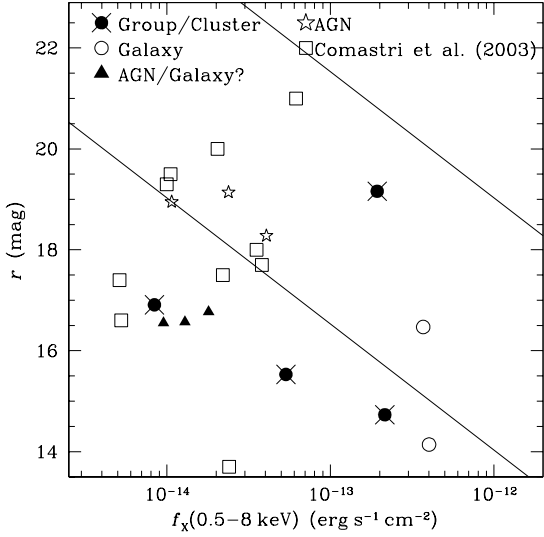


Figure 2. The X-ray to optical flux diagram for the 12 XBONGs in our sample compared to the 10 XBONGs from Comastri et al. (2003). The solid lines indicate constant X-ray-to-optical flux ratios of $\log f_X/f_{opt} = \pm 1$ and delineate the region of the parameter space occupied by powerful AGNs.

$-10^d 24^m 20^s$ and $\alpha = 23^h 54^m 5.7^s$, $\delta = -10^d 18^m 31^s$. Their luminosities in the 0.5-8 keV band are 3×10^{41} and 10^{41} erg s^{-1} respectively. The optical and X-ray properties of the remaining 12 sources are presented in Table 2. The optical spectra of the six sources which are likely to be associated with AGN (see the discussion section) are shown in Fig. 1. Clearly our selection criteria do not provide a complete sample of XBONGs that can be used for statistical studies (e.g. surface density of XBONGs). Nevertheless, our galaxies span a range of X-ray-to-optical flux ratios (see Fig. 2) similar to those probed by other XBONG samples compiled from *XMM-Newton* and *Chandra* surveys (Comastri et al. 2003), suggesting that they are representative of the XBONG population.

Four of our sources (#1, 6, 8, 10) are extended on the *XMM-Newton* images. The angular extensions of these sources correspond to 80-500 kpc implying that the X-ray emission comes from hot intracluster medium. Three more sources are galaxy cluster members. Source #2 at a redshift of $z = 0.373$ is associated with a cluster also detected by *ROSAT* while sources 11 and 12 at a redshift $z \sim 0.07$ are associated with the cluster Abell 2670; all three sources are embedded in the diffuse X-ray emission of the clusters. We note that the fluxes and luminosities for the above sources may present errors larger than those implied by photon statistics alone because of uncertainties in the background subtraction.

4 THE X-RAY SPECTRA

4.1 Hardness Ratios

In Fig. 3 we plot the hardness ratio as a function of the $g - r$ colour. The hardness ratio, HR, is defined as

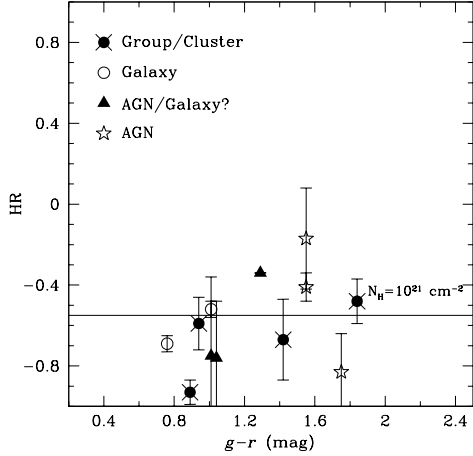


Figure 3. The hardness ratios as a function of the colour $g - r$. The solid line denotes a power-law spectrum with $\Gamma = 1.9$ and absorption $N_H = 10^{21} \text{ cm}^{-2}$ for the MOS detector. The error bars correspond to the 1σ confidence level. The point with no error bar corresponds to a 3σ upper limit (source 4).

$$\text{HR} = \frac{\text{RATE}(2080) - \text{RATE}(0520)}{\text{RATE}(2080) + \text{RATE}(0520)}, \quad (1)$$

where RATE(0520) and RATE(2080) are the count rates in the 0.5-2 and 2-8 keV spectral bands respectively. For one source (4), we have less than 5 counts in the hard band and thus we can estimate only an 3σ upper limit on the hardness ratio. The hardness ratios are estimated using the PN data except for sources that lie close to PN CCD gaps or hot pixels where we use MOS data (see section 2.2). These sources are marked in Table 2.

For comparison in Fig. 3 we also plot the line which corresponds to a power-law spectrum with photon index $\Gamma = 1.9$ and an absorbing column of $N_H = 10^{21} \text{ cm}^{-2}$ for the MOS detector. Note however, that as the MOS has a lower effective area at low energies, compared to the PN, the same hardness ratio corresponds to slightly different N_H values. The vast majority of sources present soft spectra, with values of the hardness ratio clustering around -0.5 . All sources present red colours ($g - r > 0.5$) typical of early-type systems.

4.2 Spectral Fits

Next, we attempt to constrain the spectral properties of the subsample of the 9 sources in Table 2 (sources #1, 2, 3, 6, 7, 8, 10, 11, 12) that have sufficient counts to perform X-ray spectral analysis. For the remaining sources (#4, 5, 9) poor photon statistics do not allow spectral fittings to be performed. The source spectra are extracted using a radius of 18 arcsec. In most cases, the background spectrum is estimated from nearby image regions free from sources. In the case of the sources #2, 11 and 12 which are embedded in strong cluster emission, the background was taken from adjacent regions in the cluster. Response matrices and auxiliary files are generated using the SAS tasks RMFGEN and ARFGEN respectively. We use the XSPEC v11.2 software to perform the spectral fits. The quoted errors correspond to

#	RA (J2000)	Dec (J2000)	z	Offset (arcsec)	r	f_X^3	HR	$\log f_X / f_{opt}$	L_X^4	M_r	Class ⁵	Field
1	01 53 15.2	+01 02 20	0.060	0.3	14.73	21.5	-0.93 ± 0.06^2	-1.39	2.2	-22.58	Group	ABELL267
2	02 56 30.8	+00 06 02	0.373	1.3	18.28	4.1	-0.41 ± 0.07^2	-0.21	21.5	-23.40	AGN	RXJ0256.5
3	03 01 53.9	+00 15 37	0.383	3.5	18.95	1.1	-0.15 ± 0.27^1	-1.00	6.0	-22.80	AGN	CFRS3H
4	03 38 10.0	+00 16 10	0.198	1.6	16.77	1.8	$< -0.34^1$	-1.65	2.3	-23.35	AGN/Gal?	SDSS033829
5	09 36 19.4	+61 27 21	0.131	2.3	16.55	0.95	-0.76 ± 1.0^2	-2.00	0.52	-22.62	AGN/Gal?	UGC5051
6	12 44 54.5	-00 26 39	0.231	0.8	16.91	0.84	-0.67 ± 0.20^2	-1.93	1.5	-23.60	Group	NGC4666
7	13 03 28.8	+67 26 41	0.430	2.5	19.14	2.4	-0.83 ± 0.19^1	-0.59	17.3	-22.89	AGN	ABELL1674
8	13 02 40.3	+67 28 42	0.106	1.1	15.53	5.3	-0.59 ± 0.13^1	-1.67	1.9	-23.16	Group	ABELL1674
9	13 02 51.0	+67 25 17	0.109	5.0	16.57	1.3	-0.56 ± 1.0^1	-1.87	0.46	-22.13	AGN/Gal?	ABELL1674
10	17 01 23.8	+64 14 13	0.452	1.8	19.16	19.3	-0.48 ± 0.11^2	0.34	159.7	-23.02	Group	RXJ1701.3
11	23 54 07.2	-10 25 15	0.071	3.0	16.47	36.9	-0.69 ± 0.04^2	-0.46	5.2	-21.23	Gal	ABELL2670
12	23 54 13.9	-10 25 09	0.078	2.8	14.14	40.1	-0.52 ± 0.04^2	-1.35	6.9	-23.77	Gal	ABELL2670

¹ PN, ² MOS, ³ in units 10^{-14} erg cm $^{-2}$ s $^{-1}$ (0.5-8 keV), ⁴ in units 10^{42} erg s $^{-1}$ (0.5-8 keV)⁵ Classification based on X-ray properties

Table 2. Optical and X-ray properties of the 12 XBONGs identified in this study

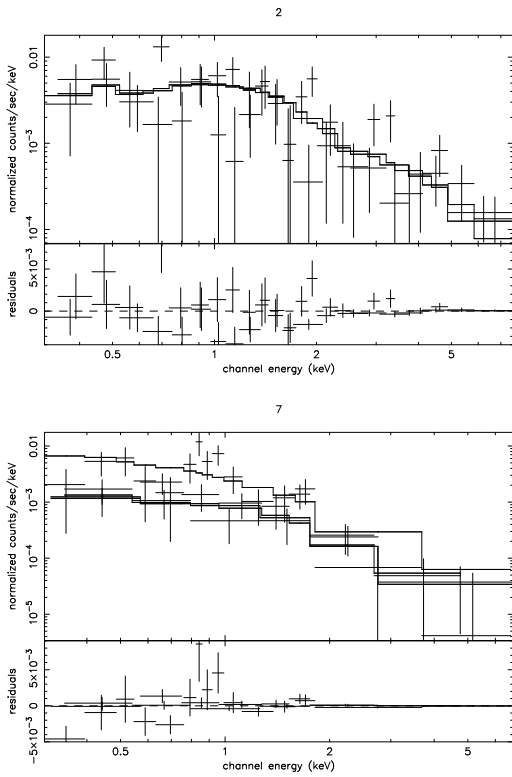


Figure 4. X-ray spectra of two candidate AGN (#2 and 7). The power-law fit to the data is shown as well together with the corresponding residuals.

the 90 per cent confidence level. The spectral fits are performed in the 0.3-8 keV band where the instruments calibration are well known. In the case of the sources #1, 6, 10, 11 and 12 we have a sufficient number of counts (more than 15 counts per bin) to perform χ^2 statistics. In the other cases (# 2, 3 7,6) where much fewer counts are observed, we use the C-statistic instead (Cash 1979) which does not require for the binning of the data. The disadvantage is that the C-statistic does not allow for the derivation of the goodness-of-fit probability unlike the χ^2 statistic.

We fit two models to the spectra: a Raymond-Smith model which provides a good representation of the hot gas emission in early-type normal galaxies, and a power-law

model which is characteristic of AGN spectra. The spectral fit results are given in Table 3. Examples of the X-ray spectra of the two X-ray brighter sources in the sample (not associated with extended X-ray emission) are shown in Figure 4. The values with no errors denote that the parameter is tied during the fitting. The column density is fixed in most cases to the Galactic value (Dickey & Lockman 1990). In the case of the Raymond-Smith model, the abundance is fixed to $Z = 0.3$. Comparison of the resulting χ^2 values of the Raymond-Smith and the power-law models (Mushotzky 1982) in the case of sources #1, 11 and 12 demonstrates that the Raymond-Smith spectrum provides a significantly better fit compared to the power-law spectrum. The best fit temperatures are ~ 1 keV typical for early-type galaxies or groups (Matsumoto et al. 1997). This strongly suggests that the X-ray emission in these objects is associated with hot gas emission. Sources #11 and 12 are not extended and thus are likely associated with gas heated by the gravitational potential of a galaxy. Sources #1 as well as 6, 8, 10 are extended and thus most likely associated with groups (#1, 6, 8) or clusters of galaxies (#10). The best fit temperature $kT \sim 1 - 3$ keV and luminosities $L_X(0.5 - 8 \text{ keV}) \sim 10^{42} - 10^{44} \text{ erg s}^{-1}$ are consistent with the above interpretation. The spectral fits for sources #2, 3 and 7 are good for both the Raymond-Smith and the power-law models. Therefore, these could be in principle associated with either normal galaxies or unobscured AGN. However, the best fit temperatures are higher (2-5 keV) than those of normal galaxies favoring, together with high X-ray luminosities, the AGN case.

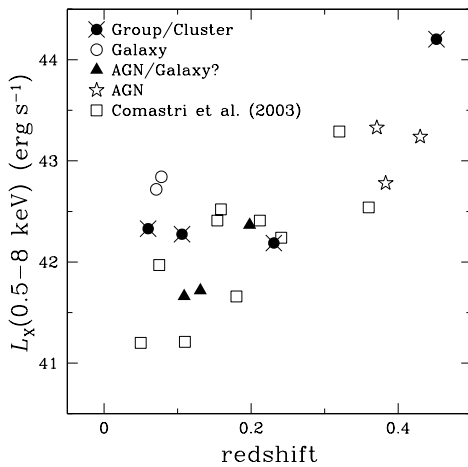
5 DISCUSSION

In this paper we explore the nature of the class of X-ray Bright Optically Inactive galaxies identified in public *XMM-Newton* fields that overlap with the SDSS. Our sample is selected in the 0.5-8 keV spectral band and comprises a total of 12 systems with $\log f_X / f_{opt} > -2$. These galaxies represent only a small fraction (1 per cent) of the full 0.5-8 keV selected catalogue totaling 1286 detections. One should bear in mind however, that our XBONGs do not constitute a complete sample as we selected only the optically brighter sources with available SDSS spectra.

A total of 8 sources are indeed, brighter than $r <$

Table 3. Spectral fits to the 9 brighter sources

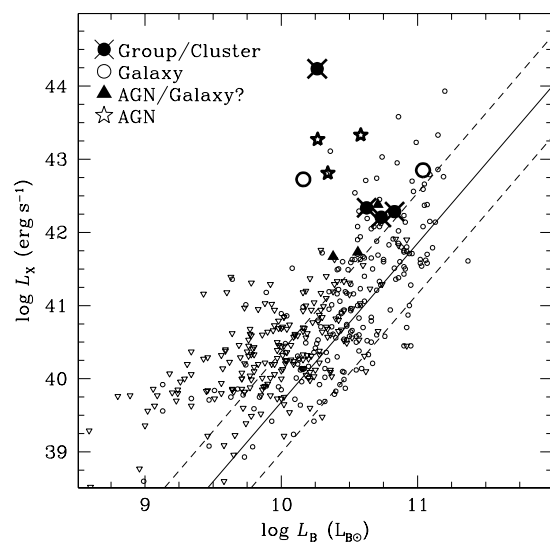
Object	Raymond-Smith			Power-Law		
	N_H^1	kT	χ^2	N_H^1	Γ	χ^2
1	9_{-5}^{+13}	$0.91_{-0.03}^{+0.05}$	97.2/92	3	$2.2_{-0.1}^{+0.1}$	400.9/94
2	7	$5.3_{-1.7}^{+2.3}$	-	7	$2.01_{-0.30}^{+0.20}$	-
3	7	$6.8_{-4.4}^{+20.7}$	-	7	$1.70_{-0.50}^{+0.55}$	-
6	1.7	$1.62_{-0.32}^{+0.42}$	113.2/107	1.7	$2.29_{-0.18}^{+0.18}$	120.9/107
7	2	$2.18_{-0.62}^{+0.95}$	-	2	$2.20_{-0.27}^{+0.30}$	-
8	2	$2.20_{-0.60}^{+1.00}$	-	2	$2.10_{-0.22}^{+0.17}$	-
10	3	$4.83_{-2.03}^{+1.99}$	43.6/63	3	$1.77_{-0.14}^{+0.14}$	42.8/63
11	3	$1.10_{-0.04}^{+0.04}$	553/594	3	$2.22_{-0.21}^{+0.09}$	716/594
12	3	$1.34_{-0.24}^{+0.71}$	451/662	3	$2.06_{-0.21}^{+0.21}$	468/662

¹ Intrinsic rest-frame column density in units of 10^{20} cm $^{-2}$ **Figure 5.** The luminosity - redshift diagram for the XBONGs in our sample compared to those from Comastri et al. (2003).

17.7 mag, the limit of the SDSS galaxy spectroscopic survey, while the remaining 4 have $17.7 < r < 19.2$ mag and are observed as part of the SDSS Luminous Red Galaxy sample. This may suggest that our sample may preferentially probe the XBONGs with a low f_X/f_{opt} . However, comparison of the $\log f_X/f_{opt}$ of our objects with the *complete* XBONG samples compiled from the XMM1dF (Fiore et al. 2003) and the *Chandra* SSA13 (Barger et al. 2001) surveys, presented by Comastri et al. (2003), does not support this claim. Indeed, as shown in Figure 2 our sources span the same range of $\log f_X/f_{opt}$ with the above XBONG samples.

Figure 5 plots the luminosity-redshift diagram for the XBONGs in the above surveys in comparison with our sample. The region probed by our sources ($10^{41} < L_X < 10^{44}$ erg s $^{-1}$, $z < 0.45$) is comparable to that probed by the objects presented in Comastri et al. (2003). The evidence above suggests that our 12 objects, although not a complete sample, provide a fair representation of the overall XBONG population.

Next we explore the origin of the X-ray emission in our sources and find that different mechanisms are in operation in different groups of objects. At least four objects (#1, 6, 8, 10) show extended X-ray emission, (> 80 kpc) with luminosi-

**Figure 6.** The $L_X - L_B$ relation for our galaxies (large symbols) in comparison with the early-type galaxy sample presented by O'Sullivan, Forbes & Ponman (2001). The small open circles and triangles represent detections and upper limits in the O'Sullivan et al. (2001) sample. The continuous line is the best fit to the O'Sullivan et al. (2001) data excluding the AGNs, Bright Cluster Galaxies and dwarfs. The dashed lines are the 1σ envelopes around the best fit.

ties $\sim 10^{42} - 10^{44}$ erg s $^{-1}$ suggesting diffuse hot gas from a cluster or group of galaxies. For the remaining sources the X-ray spectral properties provide constraints on their nature. In the case of sources #11, 12 (associated with the cluster Abell 2670) we find that a Raymond-Smith model provides a much better fit to the data compared to a power-law spectral energy distribution. The derived temperatures are ~ 1 keV, as expected for the hot gas emission encountered in the weak gravitational potentials of early-type galaxies. The X-ray luminosities are high $5 - 7 \times 10^{42}$ erg s $^{-1}$ for thermal emission. However, such high levels of X-ray emission can be encountered in massive ellipticals especially those residing in clusters (eg. Paolillo et al. 2003; O'Sullivan, Ponman & Collins 2003). This is demonstrated in Figure 6 plotting the $L_X - L_B$ for the XBONGs in our sample in comparison

with the best fit relation for early type galaxies (excluding AGNs, dwarfs and Bright Clusters Galaxies; O'Sullivan et al. 2001). Source #11 ($L_B = 1.4 \times 10^{10} L_{B\odot}$) lies well above the galaxy $L_X - L_B$ 1σ locus. This is not surprising as this source is associated with the central galaxy of the cluster and these often present enhanced X-ray emission (O'Sullivan et al. 2003). Source #12 with $L_B \approx 10^{11} L_{B\odot}$ lies marginally above the 1σ envelope in Figure 6. Three additional sources (#4, 5, 9) may be associated with normal galaxies i.e. the X-ray emission may come from X-ray binaries and hot gas rather than a supermassive black hole. In the case of these sources the poor photon statistics do not allow us to derive spectral constraints from the X-ray spectral fitting. However, the hardness ratios of these objects suggest soft spectra. The X-ray luminosities of these objects are relatively low $< 2 \times 10^{42} \text{ erg s}^{-1}$, consistent with those of normal galaxies or low luminosity AGN (eg. LINERS).

Sources #2, 3, 7 present soft X-ray spectra consistent with either a power-law or a Raymond-Smith spectrum. The power-law photon index has a value of $\Gamma \approx 2$ typical of an unobscured AGN spectrum. The best-fit temperatures in the case of a Raymond-Smith model are relatively high (2–5 keV) more typical of galaxy clusters than normal galaxies. The lack of extended X-ray emission lends no support to the galaxy cluster possibility. Furthermore, the high X-ray luminosities, $\sim 10^{43} - 10^{44} \text{ erg s}^{-1}$ render the AGN scenario very likely. This is also demonstrated in Figure 6 where the above three XBONGs deviate from the early type galaxy $L_X - L_B$ relation suggesting either AGN or cluster emission. In this case the absence of optical emission lines is puzzling. One possibility could be that the ionizing optical continuum is weak. We have estimated the 3σ upper limits for the $H\alpha$ flux using the continuum values in the SDSS spectra for all the six candidate AGNs. In the case where the $H\alpha$ is outside the spectral range, we estimate instead the $H\beta$ upper limit and we convert to $H\alpha$ using the standard Balmer decrement value of 3.1. We find that in all cases the derived $H\alpha$ to L_X upper limits are in fair agreement with the $H\alpha$ to L_X ratios estimated for Broad Line AGN (Ward et al. 1988), lending no support to the weak ionizing continuum case. Alternatively, dilution of the nuclear light by the powerful host galaxy could explain the lack of emission lines. Severgnini et al. (2003) studied a few XBONGs in the *XMM-Newton* Bright Serendipitous Source sample. They find a mixture of obscured ($N_{\text{H}} > 10^{22} \text{ cm}^{-2}$) and unobscured ($N_{\text{H}} < 10^{22} \text{ cm}^{-2}$) AGN with luminosities in the range $L_X(2 - 10 \text{ keV}) \sim 10^{42} - 10^{43} \text{ erg s}^{-1}$. They attribute the lack of emission lines to the faintness of the nucleus with respect to the galaxy. In particular, they derive that the optical nuclear flux of an AGN with an X-ray luminosity of $5 \times 10^{42} \text{ erg s}^{-1}$ can be easily outshined by a host galaxy brighter than $M_R = -22$. This scales to $M_R + \log L_X < 20.7$ for the object to be diluted. All of our AGN candidates satisfy the above criterion, apart from #2. This source is associated with a large elliptical galaxy ($M_r = -23.4$) in a galaxy cluster. We cannot then completely exclude the possibility that this source is associated with hot gas emission from either an exceedingly luminous galaxy or a cluster subclump.

Alternative scenarios for the observed X-ray emission in sources #2, 3, 4, 5, 7, 9 include (i) BL-Lac type activity (e.g. Blair et al. 1997) and (ii) Advection Dominated Ac-

cretion Flows (ADAF; Narayan & Yi 1995; Di Matteo et al. 2000). In the case of BL-Lacs one would expect strong radio emission. However, none of our sources is detected at radio wavelengths to the limits of the FIRST (1 mJy; Faint Images of the Radio Sky at Twenty centimeters; Becker et al. 1995) or the NVSS (2.5 mJy; NRAO-VLA Sky Survey; Condon et al. 1998) surveys. Nevertheless, one of our sources (#7; not detected in the NVSS) has radio-to-optical (α_{RO}) and X-ray-to-optical (α_{XO}) two point correlation indices (Stocke et al. 1991) $\alpha_{RO} < 0.57$ and $\alpha_{XO} = 1.01$ (for details on the estimation see Georgakakis et al. 2004). On the basis of the Stocke et al. (1991) classification scheme the α_{RO} upper limit and α_{XO} value above may suggest BL-Lac activity with radio emission below the NVSS flux density limit. The α_{XO} and α_{RO} values for the remaining sources are inconsistent with BL-Lac type activity. Fossati et al. (1998) showed that the peak frequency of the BL-Lac SED is a function of the radio luminosity of these objects: less luminous systems peak at UV and soft X-ray wavelengths (High energy peak BL-Lacs), while more luminous radio sources have a peak at the infrared regime (Low energy peak BL-Lacs). Source #7 at $z = 0.430$ has an upper limit radio luminosity at 5 GHz of $\nu L_{\nu} < 4 \times 10^{40} \text{ erg s}^{-1}$ suggesting that this (if a BL-Lac) is a High energy peak BL-Lac (see Figure 7a of Fossati et al. 1998). For the remaining sources (#2, 3, 4, 5, 9) The estimated radio luminosity upper limit is $\nu L_{\nu} \lesssim 5 \times 10^{39} \text{ erg s}^{-1}$, lower than the less luminous systems in the Fossati et al. (1998) sample.

ADAFs coupled with outflows and winds (Blandford & Begelman 1999) have been proposed to explain the hard X-ray emission of nearby elliptical galaxies (Allen, Di Matteo & Fabian 2000). We roughly estimate the ratio of the bolometric to the Eddington luminosity $L_{\text{BOL}}/L_{\text{EDD}}$ for our six candidate AGNs. We assume that the bolometric luminosity is an order of magnitude larger than the X-ray luminosity (e.g. Nicastro et al. 2003). The black hole mass and thus the Eddington luminosity is estimated from the $M_{\odot} - L_{\text{B}}^{\text{bulge}}$ luminosity relation of Gebhardt et al. (2000); the implicit assumption here is that the all six AGN are associated with early-type systems and thus $L_{\text{B}}^{\text{bulge}} \approx L_{\text{B}}$. We find that $L_{\text{BOL}}/L_{\text{EDD}} \sim 10^{-4} - 10^{-2}$ and hence in principle some of our objects could be associated with ADAFs. However, the ADAF models predict relatively hard X-ray spectra ($\Gamma \approx 1.4$) that are inconsistent with the soft X-ray spectral properties of most of our sources. ADAF models (e.g. Quataert & Narayan 1999) further predict that the X-ray luminosity is about 1-2 dex higher than the radio luminosity. For our sources however, the X-ray-to-radio luminosity ratio is estimated to be $> 10^3$, disfavoring the ADAF scenario.

Comastri et al. (2002) argue on the basis of the multi-wavelength observations that the XBONG *Chandra* source 031238.9-765134 could be associated with a completely hidden AGN. This source presents a flat spectrum with $\Gamma \approx 1.10 \pm 0.35$. The absence of a narrow-line emission optical spectrum typical of obscured AGN could be explained if the source were *spherically* covered by the obscuration screen, instead of the toroidal obscuration model which is usually assumed by the AGN unification models. Alternatively, Moran et al. (2002) propose that at higher redshifts ($z > 0.1$) the low equivalent width narrow emission lines may be readily masked by the optical galaxy continuum. The possibility

that a population of hidden AGN is hosted in apparently normal galaxies is intriguing. This could partially explain the scarcity of obscured AGN in the deep *Chandra* surveys. However, in our sample, we find no significant evidence for flat X-ray spectra or equivalently large absorbing columns. We note again however, that our sample may be biased against such heavily obscured sources, as it is selected in the total 0.5-8 keV band. Indeed, as the effective area of *XMM-Newton* is high at soft energies, the total energy band contains a large number of soft sources and hence, the *fraction* of absorbed XBONG may be low. Our sample is further biased against high f_X/f_{opt} objects as it is selected to contain optically bright sources with spectroscopic information available in SDSS. We nevertheless believe that the latter does not introduce any bias against obscured XBONG. At relatively low redshifts ($z \approx 0.4$) a large absorbing column will reduce the X-ray emission relative to the optical and results in low f_X/f_{opt} values; for example the source 031238.9-765134 (Comastri et al. 2002) has $\log f_X/f_{opt} \approx -1$. Interestingly, the hard to soft band flux ratios of many XBONG in the sample of Comastri et al. (2003), especially those selected in the *XMM-Newton* fields, are consistent with soft X-ray spectra (see their Fig. 4).

6 CONCLUSIONS

We explore the X-ray properties of a sample of 12 X-ray bright optically inactive galaxies (XBONG). These are detected in 20 *XMM-Newton* fields in the total 0.5-8 keV band overlapping with the SDSS. We concentrate only on those systems with available SDSS optical spectroscopic information and select sources which present only absorption lines in their optical spectra. We further select our objects to have high X-ray to optical flux ratios ($f_X/f_{opt} > -2$) to reduce contamination by normal galaxies. The resulting sample covers the luminosity range $L_X(0.5 - 8 \text{ keV}) = 5 \times 10^{41} - 2 \times 10^{44} \text{ erg s}^{-1}$ and the redshift interval $0.06 < z < 0.45$. Our sample comprises (i) extended X-ray sources most probably associated with galaxy clusters, (ii) normal galaxies and (iii) *unobscured* AGN. The unobscured AGN do not present emission lines probably because the optical light from the nucleus is diluted by a strong galaxy component (e.g. Moran et al. 2002; Severgnini et al. 2003, Georgantopoulos et al. 2003). Previous work (Comastri et al. 2002) has suggested that the lack of optical emission lines in XBONGs could be attributed to the fact that the central source suffers from large obscuration. We find no evidence in our sample for the presence of XBONGs which present significant X-ray absorption. As we imposed a cut-off in optical magnitude, our sample is not complete and therefore we cannot conclusively rule out the possibility that some XBONGs fainter than our magnitude limit present X-ray absorption. Nevertheless, our present work shows that the absence of optical emission lines in at least a fraction of XBONGs, can be explained from the dilution rather than absorption of the optical nuclear light.

7 ACKNOWLEDGMENTS

This work is jointly funded by the European Union and the Greek Ministry of Development in the framework of

the Programme 'Competitiveness – Promotion of Excellence in Technological Development and Research – Action 3.3.1', Project 'X-ray Astrophysics with ESA's mission XMM', MIS-64564.

Funding for the creation and distribution of the SDSS Archive has been provided by the Alfred P. Sloan Foundation, the Participating Institutions, the National Aeronautics and Space Administration, the National Science Foundation, the U.S. Department of Energy, the Japanese Monbukagakusho, and the Max Planck Society. The SDSS Web site is <http://www.sdss.org/>. The SDSS is managed by the Astrophysical Research Consortium (ARC) for the Participating Institutions. The Participating Institutions are The University of Chicago, Fermilab, the Institute for Advanced Study, the Japan Participation Group, The Johns Hopkins University, Los Alamos National Laboratory, the Max-Planck-Institute for Astronomy (MPIA), the Max-Planck-Institute for Astrophysics (MPA), New Mexico State University, University of Pittsburgh, Princeton University, the United States Naval Observatory, and the University of Washington.

REFERENCES

Alexander D. M., Brandt W. N., Hornschemeier A. E., Garmire G. P., Schneider D. P., Bauer F. E., Griffiths R. E., 2001, AJ, 122, 2156
 Alexander D. M. et al. 2003, AJ, 126, 539
 Allen S. W., Di Matteo T., Fabian A. C., 2000, MNRAS, 311, 493
 Barger A. J., 2001, AJ, 121, 662
 Becker R. H., White R. L., Helfand D. J., 1995, ApJ, 450, 559
 Blair A. J., Georgantopoulos I., Stewart G. C., 1997, MNRAS, 289, 921B
 Blandford R. D., Begelman M. C., 1999, MNRAS, 303L, 1
 Brandt W. N. et al., 2001, AJ, 122, 2810
 Cash W., 1979, ApJ, 228, 939
 Comastri A., Setti G., Zamorani G., Hasinger G., 1995, A&A, 296, 1
 Comastri A. et al., 2002, ApJ, 571, 771
 Comastri A., Brusa M., Mignoli M., 2003, AN, 324, 28
 Condon J. J., Cotton W. D., Greisen E. W., Yin Q. F., Perley R. A., Taylor G. B., & Broderick J. J. 1998, AJ, 115, 1693
 Dickey J. M., Lockman F. J., 1990, ARA&A, 28, 215
 Di Matteo T., Quataert E., Allen S. W., Narayan R., Fabian A. C., 2000, MNRAS, 311, 507
 Downes A. J. B., Peacock J. A., Savage A., Carrie D. R., 1986, MNRAS, 218, 31
 Elvis M., Schreier E. J., Tonry J., Davis M., Huchra J. P., 1981, ApJ, 246, 20
 Fiore F., et al. 2003, A&A, 409, 79
 Fossati G., Maraschi L., Celotti A., Comastri A., Ghisellini G., 1998, MNRAS, 299, 433
 Fukugita M., Ichikawa T., Gunn J. E., Doi M., Shimasaku K., Schneider D. P., 1996, AJ, 111, 1748
 Gebhardt, K. et al. 2000, ApJ, 543, L5
 Georgakakis A. et al. 2004, MNRAS, 349, 135
 Georgantopoulos I., Zelas A., Ward M. J., 2003, ApJ, 584, 129
 Giacconi R., et al. 2002, ApJS, 139, 369
 Griffiths R. E., Georgantopoulos I., Boyle B. J., Stewart G. C., Shanks T., della Ceca R., 1995, MNRAS, 275, 77
 Hornschemeier A. E. et al., 2001, ApJ, 554, 742
 Hornschemeier A. E. et al., 2003, AJ, 126, 575
 Maiolino R. et al. 2003, MNRAS, 344, L59
 Matsumoto H., Koyama K., Awaki H., Tsuru T., Loewenstein M., Matsushita K., 1997, ApJ, 482, 133

Moran E. C., Helfand D. J., Becker R. H., White R. L., 1996, *ApJ*, 461, 127

Moran E. C., Filippenko A. V., Chornock R., 2002, *ApJ*, 579, L71

Mushotzky R. F., 1982, *ApJ*

Mushotzky R. F., Cowie L. L., Barger A. J., Arnaud, K. A., 2000, *Nature*, 404, 459

Narayan R., Yi I., 1995, *ApJ*, 452, 710

Nicastro, F., Martocchia, A., Matt, G., 2003, *ApJ*, 589, L13

O'Sullivan E., Ponman T.J., Collins R.S., 2003, *MNRAS*, 340, 1375

O'Sullivan E., Forbes D. A., Ponman. T. J., 2001, *MNRAS*, 328, 461

Paolillo M., Fabbiano G., Peres G., Kim D.W., 2003, *ApJ*, 586, 850

Quataert E., Narayan R., 1999, *ApJ*, 520, 298

Severgnini P. et al., 2003, *A&A*, 406, 483

Stoughton C., et al., 2002, *A&AS*, 34, 1288

Strüder L., Briel U., Dennerl K., et al. 2001, *A&A*, 365, L18

Turner M. J. L., Abbey A., Arnaud M., et al., 2001, *A&A*, 365, L27.

Ward, M.J., Done, C., Fabian, A. C., Tennant, A.F., Shafer, R.A., 1988, *ApJ*, 324, 767

York D. G., et al., 2000, *AJ*, 120, 1579